THE JOURNAL OF PHYSICAL CHEMISTRY LETTERS
A JOURNAL OF THE AMERICAN CHEMICAL SOCIETY

pubs.acs.org/JPCL

Letter

Controlling Charge Carrier Lifetime in Defective WSe_2 Monolayer through Interface Engineering: a Time-Domain Ab Initio Study

Amine Slassi,* Reda Moukaouine, Jérôme Cornil, and Anton Pershin*

Cite This: *J. Phys. Chem. Lett.* 2025, 16, 1931−1938

Read Online

ACCESS | Metrics & More | Article Recommendations | Supporting Information

ABSTRACT: Trap states induced by chalcogenide vacancies in defective transition metal dichalcogenide (TMDs) monolayers are detrimental to both the charge carrier lifetime and device efficiency. To address this, chemically functionalizing the surface of defective TMD monolayers is crucial. Experimental methods such as thiol grafting on chalcogenide vacancies, oxygen passivation, and the physisorption of electroactive molecules have been explored for defect healing. Our study, using ab initio time-domain density functional theory and nonadiabatic molecular dynamics, shows that C_{20} molecular adsorption and oxygen passivation effectively mitigate nonradiative electron−hole recombination and enhance carrier charge lifetime in defective WSe_2 beyond that of pristine WSe_2 monolayers. These improvements stem from the combined effects of energy gap variations, nonadiabatic coupling, and decoherence time, resulting from either hole-trap-assisted processes or direct interactions between free electrons and holes. Our findings suggest that healing chalcogenide vacancies in defective TMDs enables precise control over charge carrier lifetime, advancing defect engineering in 2D materials.

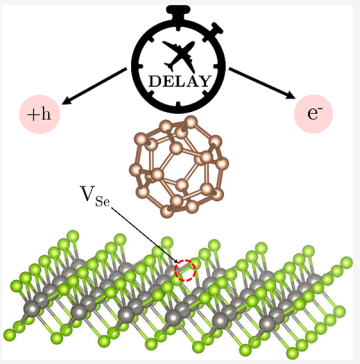

Two-dimensional transition metal dichalcogenides (TMDs) are highly promising materials for advanced optoelectronic devices such as solar cells,[1] light-emitting diodes,[2] and field-effect transistors (FETs).[3] The layered structure of 2D-TMDs consists of a transition metal layer (Mo or W) between two chalcogen atom layers (S, Se, and Te). Defects in these materials, introduced during fabrication processes, can greatly impact their functionality and performance, affecting properties like photoluminescence and field-effect mobility.[4−8] For instance, in defective MoS_2, the photoluminescence spectrum intensity can be diminished by a factor of 10^4,[9] and the field-effect mobility in devices may fall short of the theoretical value by an order of magnitude.[10] Despite their drawbacks, defects can also be utilized for functionalization,[11] activation of catalytic processes,[5] and the realization of 2D qubits.[12] Consequently, intentional generation of defects in 2D TMDs, such as through ion bombardment,[5,6,8] has become a widespread practice. Both experimental and theoretical investigations have consistently revealed that chalcogenide vacancies stand out as the dominant and energetically most favorable point defects in TMDs.[4,13,14] First-principles calculations predicted the formation of localized trap states within the band gap of MoS_2 due to sulfur vacancies,[15] which was subsequently validated in experiments.[16]

Modulating the lifetime of excited electrons and holes, dictated by the electron−hole (e-h) recombination process, is crucial for customizing TMDs for specific applications. Time-resolved spectroscopy studies on WSe_2 have shown electron lifetimes in the range of several hundred picoseconds and up to 200 ns for bound excitons.[8] On the theoretical side, ab initio time-dependent density functional theory (TDDFT) combined with nonadiabatic molecular dynamics (NAMD) simulations has emerged as a highly predictive methodology for elucidating the e-h recombination dynamics in TMD monolayers.[17,18] This approach has notably showcased that various point defects play a key role in diminishing the exciton lifetime by acting as e-h recombination centers.[15−17]

Strategies such as molecular functionalization have been successful in improving transport and optical performance of TMD-based devices by rectifying point defects.[5,11] For instance, the grafting of thiol molecules, wherein the thiol group passivates sulfur or selenium vacancies (V_{Se}) in defective MoS_2 and WSe_2, respectively, has proven to be efficacious in healing trap states.[11,19] Oxygen can also passivate chalcogen vacancies, improving electronic structure.[4,20−22] Specifically, Lu et al. demonstrated a remarkable ∼400-fold enhancement in the conductivity of WSe_2 monolayers and a ∼150-fold improvement in their photoconductivity through isoelectronic substitutional oxygen.[20] Similarly, Cai et al. theoretically predicted the efficacy of TCNQ molecule physisorption on defective MoS_2 monolayers in neutralizing detrimental trap

Received: December 30, 2024
Revised: February 6, 2025
Accepted: February 11, 2025
Published: February 17, 2025

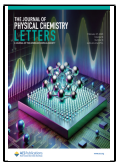

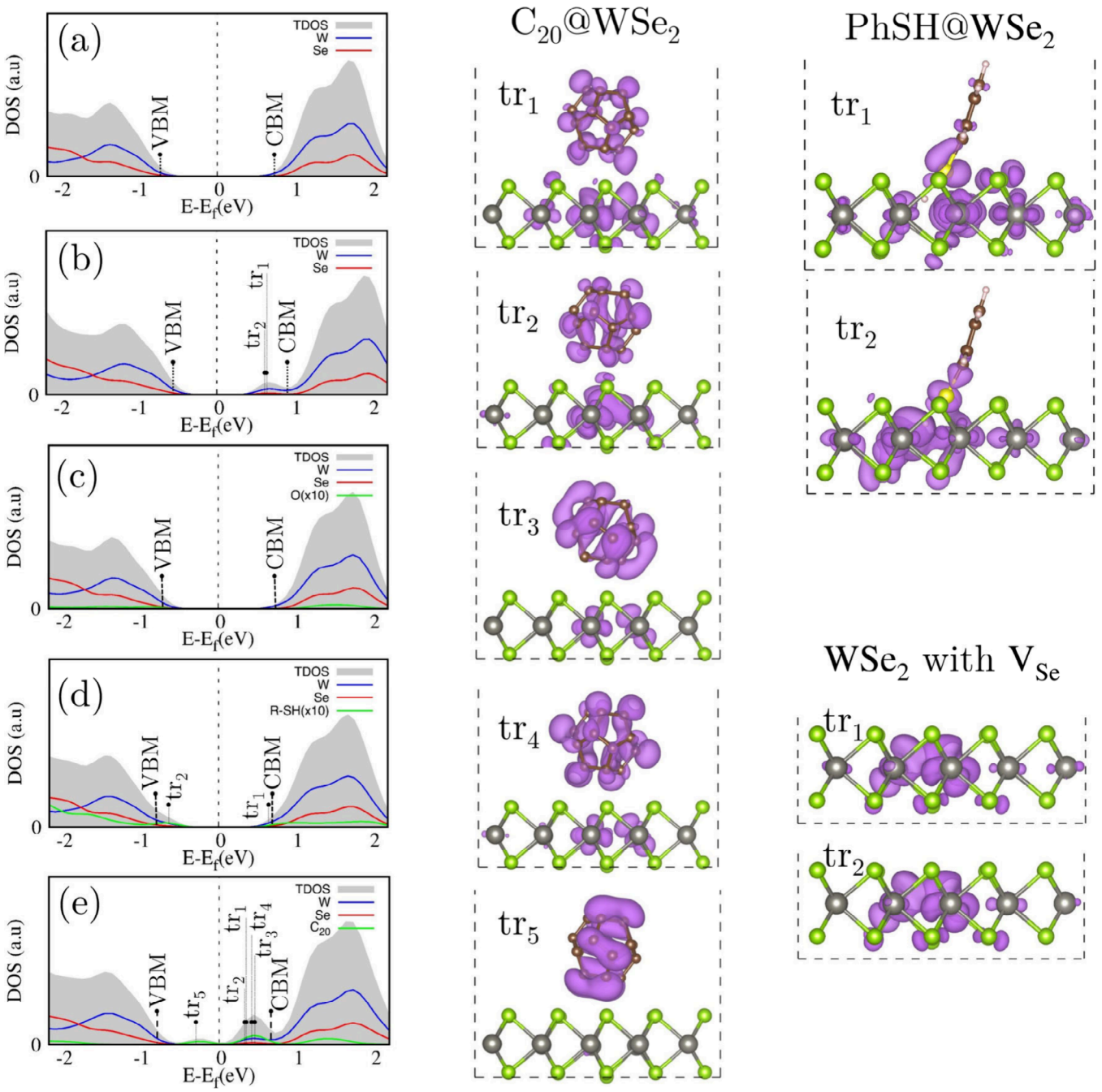

Figure 1. Total and partial density of states, calculated at the equilibrium geometries for (a) pristine WSe_2, (b) defective WSe_2 with a Se-vacancy, (c) O-substituted WSe_2, (d) thiophene grafted on WSe_2, and (e) C_{20} adsorbed on defective WSe_2, along with the charge density distributions of trap states. The VBM and CBM levels are shown in Figure S1.

states within the band gap, rendering them electrically inert.[23] In addition, molecular adsorption on defective WSe_2 has also been shown to modulate the spatial localization of V_{Se} trap states.[11]

In this paper, we focus on nullifying or alleviating the adverse effects of trap states to enhance the optical properties of defective WSe_2, representing TMD monolayers, through chemical functionalization. While previous studies have primarily utilized static density functional theory to elucidate the principal mechanisms underlying defect state healing in WSe_2 and other TMD monolayers, understanding the relationship between defect healing and the lifetime of excited charge carriers is crucial for rationalizing the potential applications of WSe_2 in optoelectronic devices. However, the impact of chemical functionalization on active defects and its subsequent effect on charge carrier lifetimes remains poorly understood. This knowledge gap has motivated the present study, employing time-domain density functional theory coupled with nonadiabatic molecular dynamics, to unravel this effect. With this approach, we aim to contribute to the comprehension of mechanisms underlying the enhancement of exciton lifetimes upon functionalization, which cannot be easily grasped within a static framework.

The NAMD simulations were conducted utilizing the decoherence induced surface hopping (DISH) method,[24,25] implemented in the Hefei-NAMD code.[26] Structural opti-

https://doi.org/10.1021/acs.jpclett.4c03723
J. Phys. Chem. Lett. 2025, 16, 1931−1938

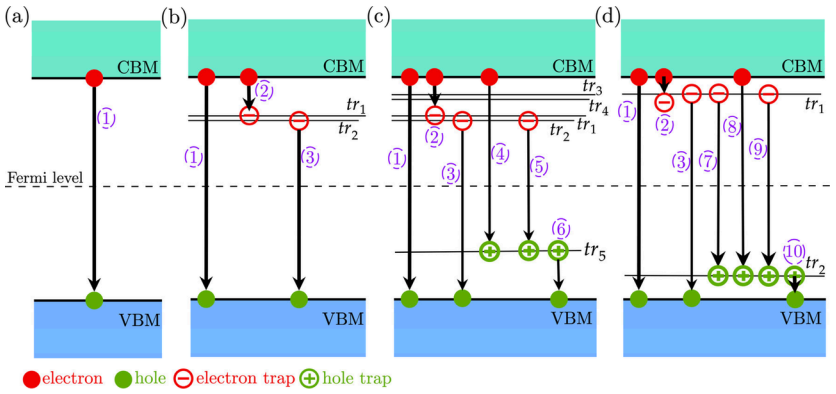

Figure 2. Possible nonradiative recombination processes, involving the defect and molecular levels, plotted for (a) pristine WSe_2, (b) defective WSe_2, (c) C_{20} adsorbed on defective WSe_2, and (d) thiol grafted on defective WSe_2. In the ground state, the levels below the Fermi energy are fully occupied, while those above the Fermi energy are empty. Note that the electronic structure of the O-substituted WSe_2 is equivalent to that of (a).

mizations, electronic structures, and ground-state molecular dynamic trajectories were computed using the Vienna ab initio simulation package (VASP).[27] The ion-electron interaction was treated with the projector augmented wave (PAW) method,[28] employing the generalized gradient approximation (GGA) with the Perdew–Burke–Ernzerhof (PBE) functional.[29] van der Waals interactions were accounted for using Grimme's DFT-D2 dispersion correction scheme.[30] To ensure accuracy of the latter, we also examined the equilibrium geometries using the vdW-DF exchange-correlation functional.[31] A cutoff energy of 450 eV for the plane-wave basis sets was maintained throughout all of the calculations.

Defective and functionalized WSe_2 were modeled in $5 \times 5 \times 1$ and $6 \times 6 \times 1$ WSe_2 supercells, including a vacuum layer of 20 Å in the z direction to eliminate spurious interactions between the periodic images. Defective WSe_2 structures were generated by removing one Se atom from the $5 \times 5 \times 1$ and $6 \times 6 \times 1$ WSe_2 supercells, resulting in a Se-vacancy concentration of 2% and 1.4%, respectively, which is rather typical for CVD and CVT grown samples.[32] Defect state healing in WSe_2 was achieved through oxygen substitution of the Se vacancy, thiophenol molecule grafting, or C_{20} molecular adsorption. The first Brillouin zone was sampled with a $5 \times 5 \times 1$ k-point mesh for electronic structure or at the Gamma point in the molecular dynamics calculations. The geometries were relaxed until the total energy and Hellmann–Feynman forces reached thresholds of 10^{-6} eV and 0.02 eV/Å, respectively. To evaluate the localization of orbital states in the material, we calculated the inverse participation ratio (IPR_i) associated with single particle orbitals $\psi_i(r)$. by the following equation:[33]

$$\mathrm{IPR}_i = \frac{\int |\psi_i(r)|^4 \, \mathrm{d}r}{\left(\int |\psi_i(r)|^2 \, \mathrm{d}r\right)^2} \tag{1}$$

Similarly, to access the localization of phonons, we calculated the phonon participation ratio (PPR) as Σq^4, where q is the atomic displacement of each atom in the Cartesian basis.[34] The radiative lifetime, τ_{rad}, is computed as follows:

$$\frac{1}{\tau_{\mathrm{rad}}} = \frac{n_{\mathrm{D}} E_{\mathrm{ZPL}}^3 \mu^2}{3\pi \in_0 c^3 \hbar^4} \tag{2}$$

where ϵ_0 is the vacuum permittivity, $\hbar$ is the reduced Planck constant, c is the speed of light, an n_D of 3.5 is the refractive index of WSe_2 at the transition energy,[35] E_{ZPL} is the zero-phonon line energy, and μ is the optical transition dipole moment.

The equilibrium structures were heated to 300 K over 7 ps by using a velocity scaling approach for equilibration. Subsequently, MD trajectories of 10 ps were generated in a microcanonical ensemble (NVE) with a time step of 1 fs. To model the quantum dynamics of electron–hole recombination on a sufficiently long time scale, the nonadiabatic (NA) couplings were computed for 5000 geometries. This was repeated 200 times in the DISH simulations, resulting in a total simulation time of 1 ns with variable initial conditions under the classical path approximation.

Before exploring dynamic calculations, we first examine the equilibrium geometries and static electronic configurations of the pristine and functionalized defective WSe_2 monolayers. Our focus is on three distinct passivating methodologies,

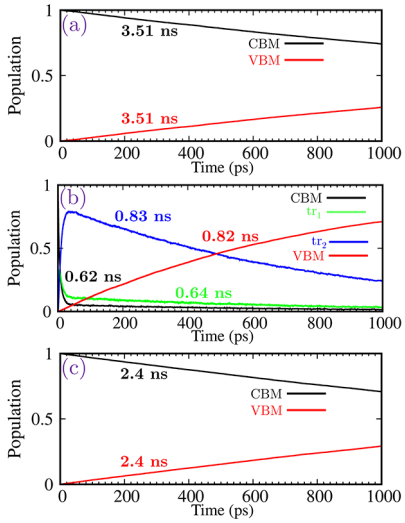

Figure 3. Charge carrier trapping and recombination dynamics in a $6 \times 6 \times 1$ (a) pristine WSe_2 monolayer, (b) Se vacancy in WSe_2, and (c) O-passivated Se vacancy in WSe_2. The time scales of the electron population for each state are obtained by fitting the data with an exponential function, $P(t) = A \times \exp[-t/\tau] + B$. Here, τ is the electron–hole recombination lifetime, shown in the plots. The results for the $5 \times 5 \times 1$ supercell are depicted in Figure S4 in the SI.

https://doi.org/10.1021/acs.jpclett.4c03723
J. Phys. Chem. Lett. 2025, 16, 1931–1938

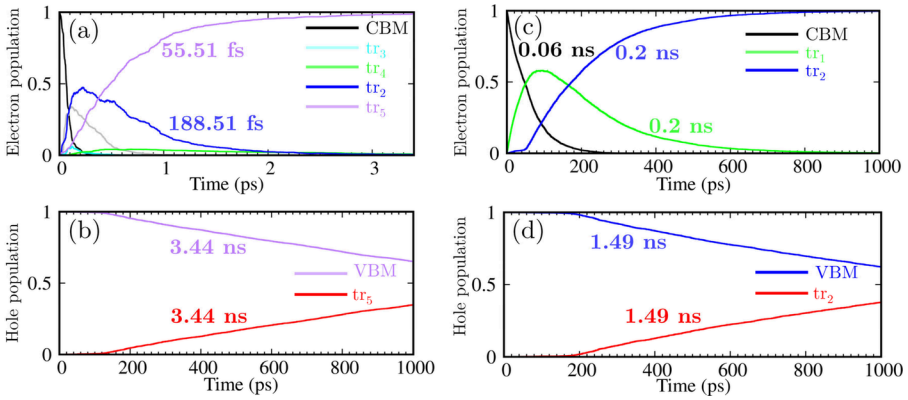

Figure 4. Charge carrier trapping and recombination dynamics in molecular healing of 6 × 6 × 1 defective WSe_2 supercell, involving (a) electron and (b) hole dynamics for C_{20} adsorption. (c and d) Electron and hole dynamics for thiol grafting, respectively. The results for the 5 × 5 x 1 supercell are depicted in Figure S5 in the SI.

mirroring recent experimental works: substitution of a Se vacancy with an oxygen atom, grafting of a thiophenol molecule, as well as the adsorption of a C_{20} molecule, which is capable of hybridizing with the defect levels.[36] Following atomic relaxation, the equilibrium geometries of all systems are presented in Figure 1 (see also Figures S1 and S2), revealing an absence of significant alterations to the basal structure of the WSe_2 monolayer induced by the various passivation strategies. Importantly, we calculated the interlayer distance between C_{20} and defective WSe_2 to be 2.64 Å and an adhesion energy of 0.70 eV, both in close agreement with the values obtained using the vdW-DF functional.[36]

Furthermore, Figure 1 shows the projected density of states for each system, alongside orbital distributions for the conduction band minimum (CBM), valence band maximum (VBM), and trap states within the band gap, as shown also in Figure S3 in the SI. For the pristine WSe_2 monolayer, the direct bandgap of 1.49 eV was computed at the K-point, closely matching photoluminescence (PL) measurements[37] and other theoretical calculations.[38] The calculated band gap of a pristine WSe_2 monolayer at the HSE06 level is 2.04 eV.[36] This value is higher by about 0.55 eV than the band gap value of 1.49 eV obtained at the level of GGA-PBE. However, combining the HSE06 and the spin−orbit coupling (SOC) decreases the band gap by about 0.34; error cancellation thus ensures a reasonable estimation of the band gap by the PBE functional. The calculated inverse participation ratio (IPR) revealed a low value of 0.04 for both the VBM and CBM states, indicating high delocalization. Figure 1b illustrates that a Se vacancy introduces two degenerate empty states, tr_1 and tr_2, within the band gap, localized at 0.32 eV below the CBM, consistent with prior theoretical calculations.[36] The two trap states with IPRs of 0.49 are spatially localized on the atoms surrounding V_{Se} and play the key role in charge trapping and electron−hole recombination in defective WSe_2. Passivation of the Se vacancy with substitutional oxygen eliminates trap states within the band gap, essentially restoring the electronic structure of pristine WSe_2, see Figure 1c. Thiophenol passivation partly restores the electronic structure of pristine WSe_2, with significant shifts of the tr_1 and tr_2 states within the band gap. More specifically, the tr_1 state shifts upward, localizing at 0.1 eV below the CBM, while tr_2 becomes fully occupied, localizing at 0.3 eV above the VBM. In addition, thiol passivation significantly alters charge density distribution for the VBM and CBM, with IPR values increasing to 0.18 for VBM and 0.17 for CBM, see Figure 1d. This suggests pronounced localization at the band edges due to hybridization with trap states. In turn, C_{20} adsorption has a pronounced effect on a trap state localization, reducing IPR values by 34% for both tr_1 and tr_2. This reduction implies that C_{20} molecular levels contribute to delocalization of the trap states from V_{Se}.

The possible mechanisms of the electron−hole recombination process, mediated by the trap states, are illustrated in Figure 2. Initially, an electron is excited from the VBM to CBM, thereafter recombining with a hole in the VBM either directly or via intermediate trap states. Typically, if the electron recombines with a hole in the valence band, the resulting carrier charge is neutralized, rendering it incapable of contributing to photocurrent within the system. However, if an electron becomes trapped within states residing within the band gap, it is effectively sequestered from participating in current flow, but a hole persists in the valence band, enabling conduction of current. Consequently, the overall current is only partly diminished rather than completely nullified.

Figure 3 shows the time-resolved populations of the states, central to the dynamics of electron−hole recombination across the three systems of interest. In the pristine WSe_2 monolayer, the direct electron−hole recombination lifetime (process 1 in Figure 2a) spans approximately 3.51 ns, aligning with experimentally observed recombination times in the range of several hundred picoseconds.[8,39] Figure 3b reveals that a V_{Se} defect significantly accelerates the nonradiative electron−hole recombination by a factor of 4.29. This is evidenced by a shortened time scale of 0.82 ns for the valence band, compared to the pristine WSe_2 monolayer. This acceleration can be attributed to the increased population of trap states, facilitating faster electron relaxation through transitions across smaller energy gaps. Consequently, trap-assisted charge recombination emerges as the predominant pathway in the defective WSe_2 monolayer. A parallel mechanism has been documented for the S vacancy in the MoS_2 monolayer,[40] as well as for the Se vacancy in $MoSe_2$ and $ReSe_2$ monolayers.[18,41]

Figure 3c shows that passivation of V_{Se} by oxygen significantly decelerates the e-h recombination by a factor of 2.92 compared to the defective monolayer, with a time scale increasing to 2.4 ns. Interestingly, the oxygen passivation results in a suppression of the e-h recombination process closely approach the time scale of pristine WSe_2. Note that the e-h recombination does not involve any trap state within the

https://doi.org/10.1021/acs.jpclett.4c03723
J. Phys. Chem. Lett. 2025, 16, 1931−1938

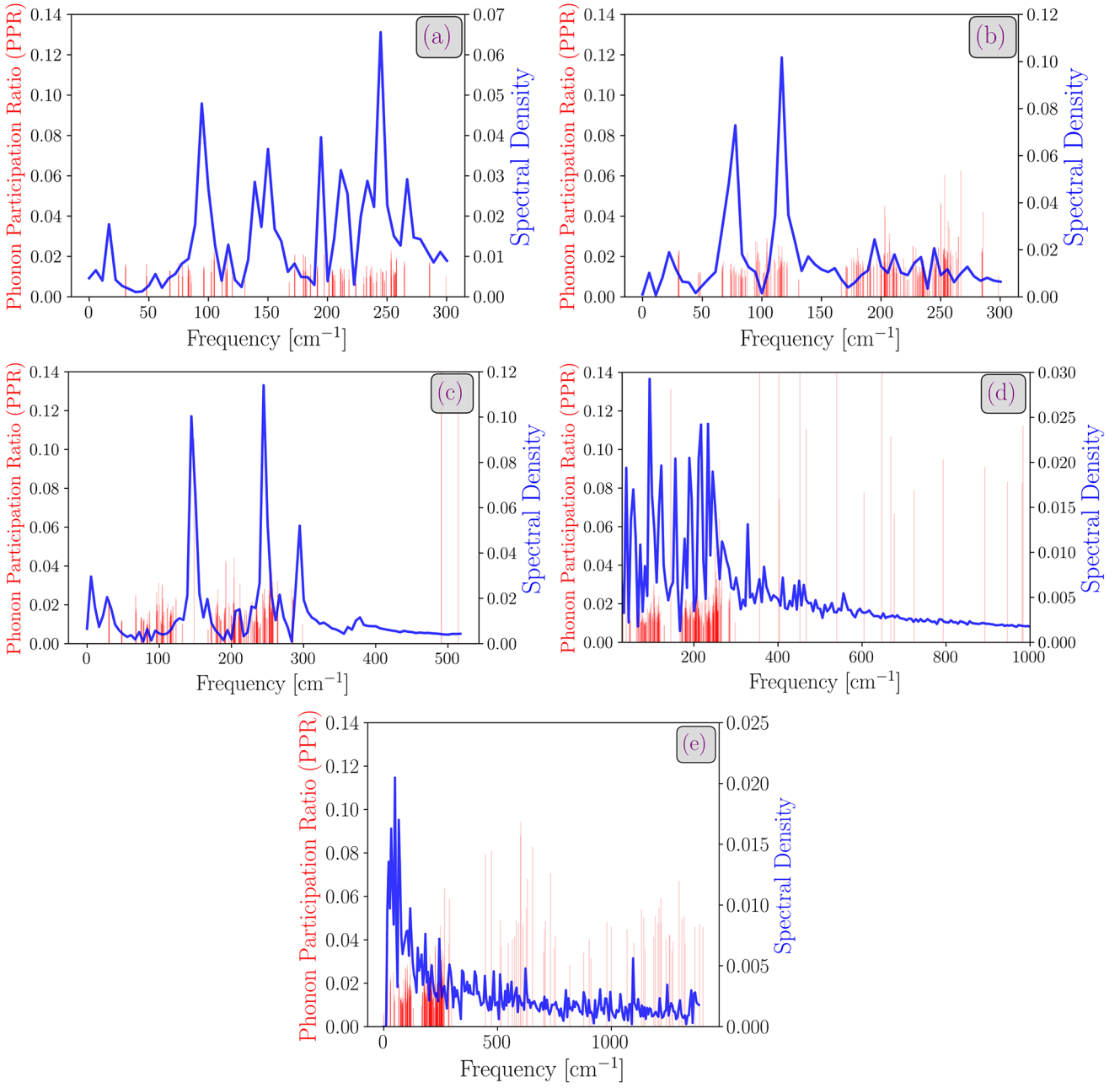

Figure 5. Spectral density associated with the variations of the energy gaps between CBM and the closest available state for an electron relaxation (either a trap state or VBM) in (a) pristine WSe_2, (b) defective WSe_2, (c) O-substituted WSe_2, (d) C_{20} adsorption on defective WSe_2, and (e) thiol grafted on defective WSe_2. The gray filled curve represents the spectral density for pristine WSe_2.

band gap, indicating a recombination mechanism similar to that of pristine WSe_2 (process 1 in Figure 2).

On the other hand, the adsorption of thiol and C_{20} molecules on defective WSe_2 results in the development of both occupied and empty states within the band gap, suggesting a different mechanism of the e-h recombination. In this regard, we consider two types of time-resolved populations: one for electrons (involving transitions between the CBM and empty trap state) and another for holes (involving transitions between higher occupied trap states and the VBM). As shown in Figure 4, the adsorption of C_{20} promotes a fast electron transition between CBM and electron-assisted traps (ET: tr_1, tr_2, tr_3, and tr_4) with a maximum population of 188 fs. This is followed by a fast transition between the ET-assisted trap and hole assisted trap state (HT) tr_5, which corresponds to the HOMO of C_{20}. In contrast, the transition of holes between the HT-assisted state and VBM occurs at a much slower rate, with a time scale of 3.44 ns, which we attribute to a lack of orbital hybridization between the tr5 level and VBM (see Figure 1). This results in a reduced e-h recombination by a factor of 1.9 with respect to V_{Se}-WSe_2, and also slightly smaller than the time scale observed in pristine WSe_2 by a factor of 0.98. In the same direction, the thiol grafting slows the nonradiative transitions. The transition from the CBM and ET tr_1 state to the higher occupied trap state tr_2 occurs at about 0.2 ns, while the transition time scale from HT tr_2 to VBM drops to 1.4 ns. This results in a significant reduction in the time scale for e-h recombination as

https://doi.org/10.1021/acs.jpclett.4c03723
J. Phys. Chem. Lett. 2025, 16, 1931−1938

compared to pristine WSe_2. For the sake of comparison, we have also performed NAMD calculations for a higher defect concentration, which quantitatively illustrate the effect concertation on the lifetime of an electron hole. The results summarized in Figures S4 and S5 as well as Table S1, demonstrated that the increase in defect concertation facilitates the nonradiative decay process.

To gain deeper insight into the electron−hole recombination process, we calculated the phonon spectral density by performing Fourier transforms of the normalized autocorrelation function (ACF) of energy gap fluctuations between relevant states. The representative time-evolutions of trap state energies are as shown in Figure S6. This analysis provides information on the phonon modes that couple to the electronic degrees of freedom.[42] The different spectral densities for pristine, defective, and healed WSe_2 monolayers are shown in Figure 5. Figure 5a shows a central peak frequency at 246 cm^{-1}, corresponding to an intense lattice vibration of the out-of-plane A_{1g} mode, which aligns with the experimentally observed central peak at 248 cm^{-1} for the out-of-plane A_{1g} mode in WSe_2.[43] The activity of this mode is diminished in defective systems, but the presence of trap states allows for additional relaxation pathways. In the case of O passivation, the increased activity of the A_{1g} mode together with the participation of a localized oxygen-related mode at ∼150 cm^{-1} result in the reduced e-h recombination lifetime. This effect can be attributed to variations in the NACs, as summarized in Supplementary Table S1. Note that the magnitude of NAC primarily depends on the wave function overlap between the two nonadiabatically coupled electronic states, the electron−phonon coupling, as well as nuclei velocity. The delocalization of charge density of VBM and CBM leads to a NA coupling of 1.1 meV in pristine WSe_2. In the O-substituted WSe_2, the NAC is increased to 1.7 meV, which leads to an increase in radiative lifetime by a factor of 1.5, consistent with the full dynamic simulations. In the defective WSe_2, the presence of defect states, particularly tr_2 in V_{Se}-WSe_2, enables rapid trap-assisted relaxation, which is also evidenced by an increase in the NAC values. Therefore, suppressing the activity of the A_{1g} mode without creating trap states may further extend the electron−hole recombination lifetime. Additionally, we analyzed the localization of phonons by plotting the phonon participation ratios, as shown in Figure 5. Our results reveal that the majority of active modes across all five systems are delocalized bulk modes, which play a key role in initiating the nonradiative decay process.

Finally, it is important to compare the e-h recombination lifetimes with the radiative lifetimes in the five systems under investigation to account for the competing decay channels of the photoexcited charge carriers. The calculated radiative lifetime of 1.5 ns for pristine WSe_2 agrees well with the experimental value of 4 ns.[44] This lifetime is significantly shorter than the nonradiative decay times, indicating that photoluminescence is the dominant relaxation mechanism. The presence of vacancies not only accelerates nonradiative decay but also substantially reduces the radiative lifetime, as shown in Supplementary Table S2. In contrast, thiol passivation partially restores the radiative lifetime, potentially enhancing the luminescence quantum yield through functionalization. Ultimately, the O-substitution and C_{20} exhibit a near-complete restoration of the radiative lifetime, showcasing the potential for improved charge carrier dynamics in these systems.

In summary, we investigated the impact of chemical functionalization on WSe_2 to address theoretically nonradiative electron−hole recombination processes caused by vacancy defects. Our findings outline the major role of an out-of-plane A_{1g} phonon mode, observed at 246 cm^{-1}, in the recombination process in pristine WSe_2. We found that vacancy defects reduce the activity of this mode, but in-gap electronic trap states facilitate fast trap-assisted recombination. When using thiophenol to passivate the Se vacancy, we observe a small improvement in the nonradiative lifetime compared to the pristine monolayer. However, substitutional oxygen effectively passivated defect states, suppressing the activity of the A_{1g} mode without developing trap states inside the band gap. This extends the recombination lifetime closer to that of pristine WSe_2. Interestingly, the adsoption of C_{20} significantly suppresses the e-h recombination and increase their nonradiative lifetime to the value close to that of pristine WSe_2. Given the key role of out-of-plane phonons, encapsulation may further reduce nonradiative losses, which is a topic that we plan to explore in future studies.

■ ASSOCIATED CONTENT

Supporting Information

The Supporting Information is available free of charge at https://pubs.acs.org/doi/10.1021/acs.jpclett.4c03723.

Tables summarizing the values of the energy gaps, pure-dephasing times, and average absolute NACs for the pairs of electronic states as well as the radiative lifetime for the indicated systems of interest; figures showing the charge carriers trapping and recombination dynamics in a 5 × 5 × 1 supercell as well as the spectral density associated with the variations of the energy gaps between CBM and the closest available state for an electron relaxation (for a 5 × 5 × 1 supercell) (PDF)

■ AUTHOR INFORMATION

Corresponding Authors

Amine Slassi − *LIRBEM, Cadi Ayyad University, Marrakech 40000, Morocco;* orcid.org/0000-0001-5877-6045; Email: a.slassi@uca.ac.ma

Anton Pershin − *HUN-REN Wigner Research Centre for Physics, H-1525 Budapest, Hungary; Department of Atomic Physics, Budapest University of Technology and Economics, H-1111 Budapest, Hungary;* orcid.org/0000-0002-2414-6405; Email: pershin.anton@wigner.hun-ren.hu

Authors

Reda Moukaouine − *HUN-REN Wigner Research Centre for Physics, H-1525 Budapest, Hungary; György Hevesy Doctoral School, ELTE Eötvös Loránd University, Institute of Chemistry, H-1117 Budapest, Hungary;* orcid.org/0009-0001-8703-9148

Jérôme Cornil − *Laboratory for Chemistry of Novel Materials, University of Mons, 7000 Mons, Belgium;* orcid.org/0000-0002-5479-4227

Complete contact information is available at: https://pubs.acs.org/10.1021/acs.jpclett.4c03723

Notes

The authors declare no competing financial interest.

https://doi.org/10.1021/acs.jpclett.4c03723
J. Phys. Chem. Lett. 2025, 16, 1931−1938

■ ACKNOWLEDGMENTS

Research in Mons is supported by the Belgian National Fund for Scientific Research (FRS-FNRS) within the Consortium des Équipements de Calcul Intensif (CÉCI) and by the Walloon Region (ZENOBE and LUCIA Tier-1 supercomputers). J.C. is an FNRS research director. A.P. acknowledges the financial support of a János Bolyai Research Fellowship of the Hungarian Academy of Sciences. R.M. is thankful for the support of the Stipendium Hungaricum scholarship.

■ REFERENCES

(1) Vikraman, D.; Arbab, A. A.; Hussain, S.; Shrestha, N. K.; Jeong, S. H.; Jung, J.; Patil, S. A.; Kim, H.-S. Design of WSe2/MoS2 Heterostructures as the Counter Electrode to Replace Pt for Dye-Sensitized Solar Cell. *ACS Sustain. Chem. Eng.* **2019**, *7* (15), 13195−13205.

(2) Ross, J. S.; Klement, P.; Jones, A. M.; Ghimire, N. J.; Yan, J.; Mandrus, D. G.; Taniguchi, T.; Watanabe, K.; Kitamura, K.; Yao, W.; et al. Electrically Tunable Excitonic Light-Emitting Diodes Based on Monolayer WSe2 p-n Junctions. *Nat. Nanotechnol.* **2014**, *9* (4), 268−272.

(3) Wang, Y.; Slassi, A.; Stoeckel, M.-A.; Bertolazzi, S.; Cornil, J.; Beljonne, D.; Samorì, P. Doping of Monolayer Transition-Metal Dichalcogenides via Physisorption of Aromatic Solvent Molecules. *J. Phys. Chem. Lett.* **2019**, *10* (3), 540−547.

(4) Wang, Y.; Sarkar, S.; Yan, H.; Chhowalla, M. Critical Challenges in the Development of Electronics Based on Two-Dimensional Transition Metal Dichalcogenides. *Nat. Electron.* **2024**, *7* (8), 638−645.

(5) Bertolazzi, S.; Bonacchi, S.; Nan, G.; Pershin, A.; Beljonne, D.; Samorì, P. Engineering Chemically Active Defects in Monolayer MoS 2 Transistors via Ion-Beam Irradiation and Their Healing via Vapor Deposition of Alkanethiols. *Adv. Mater.* **2017**, *29* (18), 1606760.

(6) Wu, Z.; Zhao, W.; Jiang, J.; Zheng, T.; You, Y.; Lu, J.; Ni, Z. Defect Activated Photoluminescence in WSe2Monolayer. *J. Phys. Chem. C* **2017**, *121* (22), 12294−12299.

(7) Zhu, W.; Low, T.; Lee, Y.-H.; Wang, H.; Farmer, D. B.; Kong, J.; Xia, F.; Avouris, P. Electronic Transport and Device Prospects of Monolayer Molybdenum Disulphide Grown by Chemical Vapour Deposition. *Nat. Commun.* **2014**, *5* (1), 3087.

(8) Moody, G.; Tran, K.; Lu, X.; Autry, T.; Fraser, J. M.; Mirin, R. P.; Yang, L.; Li, X.; Silverman, K. L. Microsecond Valley Lifetime of Defect-Bound Excitons in Monolayer ${\mathrm{WSe}}_{2}$. *Phys. Rev. Lett.* **2018**, *121* (5), 57403.

(9) Amani, M.; Lien, D.-H.; Kiriya, D.; Xiao, J.; Azcatl, A.; Noh, J.; Madhvapathy, S. R.; Addou, R.; KC, S.; Dubey, M.; et al. Near-Unity Photoluminescence Quantum Yield in MoS2. *Science (80-.).* **2015**, *350* (6264), 1065−1068.

(10) Kaasbjerg, K.; Thygesen, K. S.; Jacobsen, K. W. Phonon-Limited Mobility in n-Type Single-Layer MoS2 from First Principles. *Phys. Rev. B* **2012**, *85* (11), 115317.

(11) Zhao, Y.; Gali, S. M.; Wang, C.; Pershin, A.; Slassi, A.; Beljonne, D.; Samorì, P. Molecular Functionalization of Chemically Active Defects in WSe 2 for Enhanced Opto-Electronics. *Adv. Funct. Mater.* **2020**, *30* (45), 2005045.

(12) Koperski, M.; Nogajewski, K.; Arora, A.; Cherkez, V.; Mallet, P.; Veuillen, J.-Y.; Marcus, J.; Kossacki, P.; Potemski, M. Single Photon Emitters in Exfoliated WSe2 Structures. *Nat. Nanotechnol.* **2015**, *10* (6), 503−506.

(13) Bussolotti, F.; Kawai, H.; Maddumapatabandi, T. D.; Fu, W.; Khoo, K. H.; Goh, K. E. J. Role of S-Vacancy Concentration in Air Oxidation of WS 2 Single Crystals. *ACS Nano* **2024**, *18* (12), 8706−8717.

(14) Ildefonso, L. M. V.; Buthers, E. L.; Archanjo, B. S.; Legnani, C.; Quirino, W. G.; Massote, D. V. P.; Maciel, I. O.; Fragneaud, B. Study of Punctual Defects in Monolayer WS 2: Evidence of Correlations Between Raman and Photoluminescence Spectroscopy. *J. Phys. Chem. C* **2024**, *128* (17), 7294−7305.

(15) Slassi, A.; Cornil, J. Theoretical Characterization of Strain and Interfacial Electronic Effects in Donor-Acceptor Bilayers of 2D Transition Metal Dichalcogenides. *2D Mater.* **2019**, *6* (1), 015025.

(16) Xie, Y.; Liang, F.; Chi, S.; Wang, D.; Zhong, K.; Yu, H.; Zhang, H.; Chen, Y.; Wang, J. Defect Engineering of MoS 2 for Room-Temperature Terahertz Photodetection. *ACS Appl. Mater. Interfaces* **2020**, *12* (6), 7351−7357.

(17) Li, L.; Long, R.; Prezhdo, O. V. Why Chemical Vapor Deposition Grown MoS 2 Samples Outperform Physical Vapor Deposition Samples: Time-Domain Ab Initio Analysis. *Nano Lett.* **2018**, *18* (6), 4008−4014.

(18) Yang, Y.; Tokina, M. V.; Fang, W.-H.; Long, R.; Prezhdo, O. V. Influence of Tungsten Doping on Nonradiative Electron-Hole Recombination in Monolayer MoSe2 with Se Vacancies. *J. Chem. Phys.* **2020**, *153* (15), 154701.

(19) Förster, A.; Gemming, S.; Seifert, G.; Tománek, D. Chemical and Electronic Repair Mechanism of Defects in MoS 2 Monolayers. *ACS Nano* **2017**, *11* (10), 9989−9996.

(20) Lu, J.; Carvalho, A.; Chan, X. K.; Liu, H.; Liu, B.; Tok, E. S.; Loh, K. P.; Castro Neto, A. H.; Sow, C. H. Atomic Healing of Defects in Transition Metal Dichalcogenides. *Nano Lett.* **2015**, *15* (5), 3524−3532.

(21) Zheng, Y. J.; Chen, Y.; Huang, Y. L.; Gogoi, P. K.; Li, M.-Y.; Li, L.-J.; Trevisanutto, P. E.; Wang, Q.; Pennycook, S. J.; Wee, A. T. S.; et al. Point Defects and Localized Excitons in 2D WSe2. *ACS Nano* **2019**, *13* (5), 6050−6059.

(22) Petö, J.; Ollár, T.; Vancsó, P.; Popov, Z. I.; Magda, G. Z.; Dobrik, G.; Hwang, C.; Sorokin, P. B.; Tapasztó, L. Spontaneous Doping of the Basal Plane of MoS2 Single Layers through Oxygen Substitution under Ambient Conditions. *Nat. Chem.* **2018**, *10* (12), 1246−1251.

(23) Cai, Y.; Zhou, H.; Zhang, G.; Zhang, Y.-W. Modulating Carrier Density and Transport Properties of MoS 2 by Organic Molecular Doping and Defect Engineering. *Chem. Mater.* **2016**, *28* (23), 8611−8621.

(24) Jaeger, H. M.; Fischer, S.; Prezhdo, O. V. Decoherence-Induced Surface Hopping. *J. Chem. Phys.* **2012**, *137* (22), 22A545.

(25) Craig, C. F.; Duncan, W. R.; Prezhdo, O. V. Trajectory Surface Hopping in the Time-Dependent Kohn-Sham Approach for Electron-Nuclear Dynamics. *Phys. Rev. Lett.* **2005**, *95* (16), 163001.

(26) Zheng, Q.; Chu, W.; Zhao, C.; Zhang, L.; Guo, H.; Wang, Y.; Jiang, X.; Zhao, J. Ab Initio Nonadiabatic Molecular Dynamics Investigations on the Excited Carriers in Condensed Matter Systems. *WIREs Comput. Mol. Sci.* **2019**, *9* (6), No. e1411.

(27) Kresse, G.; Marsman, M. *VASP the GUIDE*; Universität Wien, 2012.

(28) Kresse, G.; Joubert, D. From Ultrasoft Pseudopotentials to the Projector Augmented-Wave Method. *Phys. Rev. B* **1999**, *59* (3), 1758−1775.

(29) Perdew, J. P.; Burke, K.; Ernzerhof, M. Generalized Gradient Approximation Made Simple. *Phys. Rev. Lett.* **1996**, *77* (18), 3865−3868.

(30) Grimme, S. Semiempirical GGA-Type Density Functional Constructed with a Long-Range Dispersion Correction. *J. Comput. Chem.* **2006**, *27* (15), 1787−1799.

(31) Dion, M.; Rydberg, H.; Schröder, E.; Langreth, D. C.; Lundqvist, B. I. Van Der Waals Density Functional for General Geometries. *Phys. Rev. Lett.* **2004**, *92* (24), 246401.

(32) Choi, S. H.; Yang, S.-H.; Park, S.; Cho, B. W.; Nguyen, T. D.; Kim, J. H.; Kim, Y.-M.; Kim, K. K.; Lee, Y. H. Is Chemical Vapor Deposition of Monolayer WSe2 Comparable to Other Synthetic Routes? *APL Mater.* **2023**, *11* (11), 111124.

(33) Murphy, N. C.; Wortis, R.; Atkinson, W. A. Generalized Inverse Participation Ratio as a Possible Measure of Localization for Interacting Systems. *Phys. Rev. B* **2011**, *83* (18), 184206.

(34) Turanský, R.; Brndiar, J.; Pershin, A.; Gali, Á.; Sugimoto, H.; Fujii, M.; Štich, I. Structure and Properties of Heavily B and P

https://doi.org/10.1021/acs.jpclett.4c03723
J. Phys. Chem. Lett. 2025, 16, 1931−1938

Codoped Amorphous Silicon Quantum Dots. *J. Phys. Chem. C* **2021**, *125* (42), 23267−23274.
(35) Alzaid, M.; Hadia, N. M. A.; Shaaban, E. R.; El-Hagary, M.; Mohamed, W. S. Thickness Controlling Bandgap Energy, Refractive Index and Electrical Conduction Mechanism of 2D Tungsten Diselenide (WSe2) Thin Films for Photovoltaic Applications. *Appl. Phys. A: Mater. Sci. Process.* **2022**, *128* (2), 94.
(36) Slassi, A.; Gali, A.; Cornil, J.; Pershin, A. Non-Covalent Functionalization of Pristine and Defective WSe 2 by Electron Donor and Acceptor Molecules. *ACS Appl. Electron. Mater.* **2023**, *5* (3), 1660−1669.
(37) Li, Z.; Wang, T.; Jin, C.; Lu, Z.; Lian, Z.; Meng, Y.; Blei, M.; Gao, S.; Taniguchi, T.; Watanabe, K.; et al. Emerging Photoluminescence from the Dark-Exciton Phonon Replica in Monolayer WSe2. *Nat. Commun.* **2019**, *10* (1), 2469.
(38) Yang, Y.; Fang, W.-H.; Benderskii, A.; Long, R.; Prezhdo, O. V. Strain Controls Charge Carrier Lifetimes in Monolayer WSe 2: Ab Initio Time Domain Analysis. *J. Phys. Chem. Lett.* **2019**, *10* (24), 7732−7739.
(39) Yan, T.; Qiao, X.; Liu, X.; Tan, P.; Zhang, X. Photoluminescence Properties and Exciton Dynamics in Monolayer WSe2. *Appl. Phys. Lett.* **2014**, *105* (10), 101901.
(40) Li, L.; Long, R.; Bertolini, T.; Prezhdo, O. V. Sulfur Adatom and Vacancy Accelerate Charge Recombination in MoS 2 but by Different Mechanisms: Time-Domain Ab Initio Analysis. *Nano Lett.* **2017**, *17* (12), 7962−7967.
(41) Dou, W.; Zhang, L.; Song, B.; Hua, C.; Wu, M.; Niu, T.; Zhou, M. Vacancy-Regulated Charge Carrier Dynamics and Suppressed Nonradiative Recombination in Two-Dimensional ReX2 (X = S, Se). *J. Phys. Chem. Lett.* **2022**, *13* (45), 10656−10665.
(42) Zou, J.; Zhu, R.; Wang, J.; Meng, H.; Wang, Z.; Chen, H.; Weng, Y.-X. Coherent Phonon-Mediated Many-Body Interaction in Monolayer WSe 2. *J. Phys. Chem. Lett.* **2023**, *14* (20), 4657−4665.
(43) Jeong, T. Y.; Jin, B. M.; Rhim, S. H.; Debbichi, L.; Park, J.; Jang, Y. D.; Lee, H. R.; Chae, D.-H.; Lee, D.; Kim, Y.-H.; et al. Coherent Lattice Vibrations in Mono- and Few-Layer WSe2. *ACS Nano* **2016**, *10* (5), 5560−5566.
(44) Jin, C.; Kim, J.; Wu, K.; Chen, B.; Barnard, E. S.; Suh, J.; Shi, Z.; Drapcho, S. G.; Wu, J.; Schuck, P. J.; et al. On Optical Dipole Moment and Radiative Recombination Lifetime of Excitons in WSe 2. *Adv. Funct. Mater.* **2017**, *27* (19), 1601741.

https://doi.org/10.1021/acs.jpclett.4c03723
J. Phys. Chem. Lett. 2025, 16, 1931−1938